Article | Received 21 February 2025; Accepted 22 April 2025; Published 11 June 2025
https://doi.org/10.55092/ae20250002

Event-triggered adaptive neural network asymptotic tracking control of intelligent vehicles with composite learning

Yingjie Deng[1,2], Fangcheng Liu[2], Songtao Wang[2,*], Yifei Xu[1,2], Tao Ni[1,2] and Dingxuan Zhao[1,2]

[1] State Key Laboratory of Crane Technology, Yanshan University, Heibei, China

[2] School of Mechanical Engineering, Yanshan University, Hebei, China

* Correspondence author; E-mail: wangsongtao0427@163.com.

Highlights:

- Benefitted from composite learning, the proposed scheme takes on the better neural learning and less control conservativeness than the existing adaptive asymptotic control approaches.
- This paper opens the avenue to address the high-precision tracking of nonlinear intelligent vehicles by guaranteeing the asymptotic stability.
- Taking the advantage of ETC, the proposed scheme separately reduces the communication burden in the different controller-to-actuator channels compared with the continuous control work.

Abstract: In the current epoch of intelligent transportation, achieving high-precision tracking control for autonomous vehicles is a crucial challenge due to the presence of system nonlinearities, uncertainties, and communication constraints. Traditional continuous control methods often lead to excessive communication traffic, while existing adaptive control techniques struggle to ensure asymptotic tracking accuracy under these constraints. To address these issues, this paper investigates the problem of high-precision tracking control for intelligent vehicles by designing an event-triggered asymptotic composite neural tracking control scheme. In the proposed framework, radial basis function neural networks are employed to compensate for system nonlinearities and uncertainties. By introducing integral-bounded functions into both the control laws and adaptive laws, the asymptotic convergence of positional tracking errors is ensured through the adaptive backstepping approach. To reduce communication traffic, an event-triggered control strategy is implemented in the controller-to-actuator channel, where variable threshold-based triggering conditions are designed. Furthermore, to enhance the approximation capability of neural networks, composite learning is incorporated into the control design. A novel serial-parallel estimation model is established to generate prediction errors while simultaneously ensuring asymptotic stability. The stability of the overall system is rigorously analyzed using Lyapunov's direct method and the Barbalat lemma. Finally, numerical simulations are conducted to validate the effectiveness and superiority of the proposed control scheme.

Keywords: neural networks; composite learning; event-triggered control; intelligent vehicles; asymptotic tracking control

1. Introduction

Intelligent vehicles have drawn compelling interests due to it prominent advantages on enhancing riding comfort and traffic efficiency. Automation of intelligent vehicles is confronted with three main problems, namely sensing, path planning and motion control, among which the motion control is most underlying technology. Objective tracking and path following are deemed as the kernel problems in motion control, which are transformable by using ghost-car guidance [1]. By incorporating the modern control methods, plenty of researches have addressed the tracking and path-following problems of intelligent vehicles. To ensure the better robustness against uncertainties, the sliding mode control (SMC) was utilized in [1–5]. To deal with constraints and achieve the optimal control performance, the model predictive control (MPC) was employed in [6–8]. To realize the prescribed disturbance attenuation level, the robust H_∞ controller was fabricated in [9–13] by using linear matrix inequalities (LMIs). However, MPC requires the accurate vehicle model, which is unrealistic due to the existence of model nonlinearities and variable parameters. The H_∞ control is usually based on a linear vehicle model with assuming the constant longitudinal velocity, namely the form $\dot{x} = Ax + Bu$. This assumption inevitably limits its flexibility in sharp turns and complicated traffic. For the nonlinear vehicle model with uncertainties, SMC requires the known upper bound of uncertainties, and the chattering phenomenon must be considered. In a data-driven manner, [14] extended the model free control to a four-wheel independent steering vehicle where the model is no longer required. However, the control performance relied much on the selection of key parameters.

Benefited from the universal approximation property, the NN and the fuzzy logic system (FLS) were widely employed to deal with uncertainties in nonlinear systems [15–19]. This train of thought has also expanded to the control of intelligent vehicles in [20–23]. Nevertheless, the direct adaptive control (DAC) was incarnated into the update of NNs and FLSs in most of these researches. Although the closed-loop stability can be ensured, the interpretability of neural and fuzzy learning is insufficient. There is no doubt that the negative neural and fuzzy approximation performance consequently vitiates the control effectiveness. To mediate the balance between approximation and stability, the composite learning technique was presented for the control of nonlinear systems in [24,25], where the approximation performance of NNs and FLSs can be enhanced by utilizing the SPEM. To exempt parameter convergence from the requisite persistent excitation condition, the online-recorded data were utilized in [26–28] to instigate the interval excitation in the composite learning. The above researches concentrated more on the theoretical improvement of composite learning itself. In [25,29], researchers have explored its applications in various marine vehicles. As the intelligent vehicle usually cruises at high speeds with time-varying road loads, its model dynamics are strongly coupled and nonlinear. It is worthwhile to improve the control performance of intelligent vehicles by introducing composite learning.

Control precision is one of essentials for guaranteeing reliability of intelligent vehicles. For some specific maneuvers, such as snaking and J turn, the high tracking precision to the reference can increase the agility of intelligent vehicles and prevent from anti-rollover. From the viewpoint of stability, the asymptotic convergence of tracking errors must be preferred than the bounded results in high-precision maneuvers. However, the existing researches like [20–23,30] can only come to the bounded stability conclusions. Actually, it is challenging to reach the asymptotic stability in the adaptive neural or fuzzy control of uncertain nonlinear systems. Due to the existence of approximation errors, the introduction of NNs and FLSs leaves an inexpungible term in the Lyapunov's candidate, and thereby provokes the instability. Although the researches like [31,32] fulfilled the globally asymptotically stable observation and control in T-S fuzzy models, the fuzzy weight functions were presumed to be known or limited. Similar with H_∞ control, they also relied much on solving LMIs. Recently, by involving the $\sigma-$modification terms composed of integral-bounded functions into the control framework, it is possible to asymptotically stabilize the uncertain nonlinear systems with the adaptive backstepping approach [33]. In [34–36], the integral-bounded functions were employed to make up the robust term, which can offset input nonlinearities and exogenous disturbances asymptotically in conjunction with the Young's inequality and the hyperbolic tangent function. In [37–41], the $\sigma-$ modification with integral functions was incorporated into the update of NNs and FLSs, so as to asymptotically eliminate the unknown model dynamics lumped with the exogenous disturbances. One conspicuous drawback of these adaptive asymptotic neural and fuzzy control is that all their neural and fuzzy weights must be updated in a compact form, namely in the minimum learning parameter (MLP). Although the algorithmic computational complexity can be reduced with the aid of DAC, the MLP cannot guarantee the satisfactory approximation capacity of NNs and FLSs. Moreover, the MLP is irreconcilable with the composite learning. By all accounts, there are seldom researches addressing asymptotic stability and composite learning simultaneously. Furthermore, few researches have accommodated the adaptive asymptotic control of vehicles with the influence of uncertainties. Recently, an event-triggered adaptive neural asymptotic tracking control framework for underactuated ships was constructed recently by [42]. This framework ensures the prescribed control performance via transformation functions. However, this outcome also adopted DAC with the MLPs of NNs.

With the advent of networked industries, ETC has been a widespread concern due to its advantages in saving communication resources and alleviating network jam. ETC was commonly integrated with the adaptive backstepping in the control of uncertain nonlinear systems [43–47]. For its application, ETC was applied to the marine vehicles in [23,42,48–51], and to the land vehicles in [13,32,52,53]. Recently, ETC was assimilated into the composite learning for nonlinear systems in [54], which can reduce the transmission traffic the without compromising the neural and fuzzy approximation. This idea was also shown in [55–57] for the control of marine vehicles. However, the event-triggered composite learning was seldom fabricated for the intelligent land vehicles due to its coupled propulsion mode. Moreover, the asymptotic stability cannot be procured in the existing researches.

Motivated by the above challenges, this paper designs a uniform event-triggered asymptotic composite neural control framework for intelligent vehicles. By inserting the integral-bounded functions into the control scheme, the asymptotic stability is guaranteed. To achieve the composite learning, a novel asymptotic SPEM is constructed with a robust adaptive compensating term. Thereby, the asymptotic stable update of neural weights can be fulfilled by embedding prediction errors. By using the Lagrange's mean value theorem, the asymptotic stability and avoidance of "Zeno" behavior are both confirmed to be ensured by event-triggered conditions with variable thresholds. Compared with the existing researches, the proposed scheme mainly has three contributions:

(1) Benefitted from composite learning, the proposed scheme takes on the better neural learning and less control conservativeness than the existing adaptive asymptotic control approaches like [37–41].

(2) This paper opens the avenue to address the high-precision tracking of nonlinear intelligent vehicles by guaranteeing the asymptotic stability. Therefore, the proposed scheme outperforms the bounded results like [20–23,30] in its adaptability to tracking targets.

(3) Taking the advantage of ETC, the proposed scheme separately reduces the communication burden in the different controller-to-actuator channels compared with the continuous control work like [20–22,36–38].

The structure of the remaining part of this paper is arranged as follows. In Section 2, the basic assumptions and lemmas that underpin the subsequent theoretical derivations are presented. Section 3 introduces the mathematical model of the vehicle, which acts as the basis for control design. As the core of this work, Section 4 elaborates on the design of the proposed controller. Section 5 is dedicated to the stability analysis and proof of the closed-loop system. In Section 6, simulation experiments are carried out to compare and verify the effectiveness of the proposed method. Finally, Section 7 concludes the paper by summarizing the main findings and outlining potential future research avenues.

2. Preliminaries

This section describes some of the mathematical tools used for controller design and stability proofs below:

Assumption 1. *All variables appearing in (5), along with x_d and y_d, are bounded within a compact domain. Additionally, x_d and y_d exhibit continuous second-order differentiability.*

Assumption 2. *The pitch angle $\delta_m \neq \pm(\pi/2)$ and the heading error $|\psi_e| \leq (\pi/2)$.*

Remark 1. *For the above two assumptions, we illustrate their feasibility in real-world scenarios. (1) Compact Set. In physical systems, all variables are usually subject to physical constraints. The motion of a vehicle is finite, and velocity and acceleration cannot grow indefinitely, so it is reasonable to assume that the state variables are in a compact set. (2) Second-order Continuity. This assumption requires that the target trajectory (x_d, y_d) has continuous second-order derivatives. The smoothness of the trajectory is critical to ensure feasible control inputs. Methods such as B-spline curves, Bezier curves, or polynomial interpolation are often used to generate smooth trajectories, thus ensuring that their second-order derivatives are continuous. The reasonableness of Assumption 2 comes mainly from kinematic constraints, physical feasibility, and control stability, which can be met by the vehicle in real-world environments with reasonable motion control and sensor feedback. When $\delta_m \neq \pm\frac{\pi}{2}$ implies that the carrier is perfectly perpendicular to the ground, which is usually unrealistic; The heading error $|\psi_e| \leq \frac{\pi}{2}$ is for the sake of ensuring the correctness when calculating the course error in the coordinate system.*

Lemma 1. *For a nonlinear function $f(\bar{x}) \in \mathscr{R}^1$ defined on a compact domain, there exists an RBF neural network representation:*

$$f(\bar{x}) = \theta^T \psi(\bar{x}) + \zeta(\bar{x}) \tag{1}$$

where $\theta \in \mathscr{R}^m$ is Network weight vector. $\psi(\bar{x}) \in \mathscr{R}^m$ is Radial basis function vector. $\zeta(\bar{x}$ is approximation error with $|\zeta(\bar{x})| \leq \zeta_{\max}$. The error bound $\zeta_{\max}$ can be made arbitrarily small through optimal selection of θ and $\psi(\cdot)$.

Lemma 2. *[17] $\varphi(\bar{x})$ can be selected as Gaussian functions. If $\bar{x} = [x_1, \cdots, x_l]^{\mathrm{T}}$ and $\bar{x}_p = [x_1, \cdots, x_p]^{\mathrm{T}}$, where $p \leq l$, then the following inequality holds*

$$\|\varphi(\bar{x})\| \leq \|\varphi(\bar{x}_p)\| \tag{2}$$

Lemma 3. *[34] For any variable $s \in \mathscr{R}^1$ and a continuous function $\sigma(t)$ satisfying*

$$\sigma(t) > 0, \int_0^{+\infty} \sigma(t)\mathrm{d}t \leq \bar{\sigma} \tag{3}$$

where $\bar{\sigma}$ is a positive constant, the following inequality holds

$$|s| \leq \frac{s^2}{\sqrt{s^2 + \sigma^2(t)}} + \sigma(t) \tag{4}$$

3. Vehicle dynamics model

For vehicle's asymptotic horizontal tracking control design, the dynamic model controlled by the steering angle of the front wheels is used. According to [58], roll and pitch motion are disregarded, along with the sliding angle β, relative heading φ and tire's side slip angles.

$$\begin{cases} \dot{x} = u\cos\psi - v\sin\psi \\ \dot{y} = u\sin\psi + v\cos\psi \\ \dot{\psi} = r \\ \dot{u} = vr - fg + m^{-1}\left[(k_1 f - k_2)u^2 + T + C_f\delta(v + ar)u^{-1}\right] \\ \dot{v} = -ur + m^{-1}\left[vu^{-1}(C_f + C_r) + C_f\delta + T\delta + ru^{-1}(bC_f - aC_r)\right] \\ \dot{r} = I_z^{-1}\left[-fmhur + vu^{-1}(bC_r - aC_f) - ru^{-1}(b^2C_f - a^2C_r) + aC_r\delta + aT\delta\right] \end{cases} \tag{5}$$

where u denotes the longitudinal velocity, v denotes the lateral velocity, r is the yaw rate, T denotes the traction and/or braking force, δ denotes the steering angle, ψ denotes the heading angle. Respectively, other parameters and their description are defined in the Table 1.

Control Objective: Design the control inputs T and δ for the virtual target at (x_d, y_d), such that (x, y) in (5) can asymptotically track (x_d, y_d).

Table 1. Vehicle model parameters.

Symbol	Description	Value
m	Mass of the full vehicle	1480 kg
h	Height from center of gravity to road	0.53 m
I_z	Initial moment around z-axis	2350 kg·m^2
g	Acceleration of gravity force	9.81 m/s^2
f	Rotating friction coefficient	0.02
a	Distances from front tyres to center of gravity	1.05 m
b	Distances from rear tyres to center of gravity	1.63 m
C_f	Cornering stiffness coefficients of front tyres	135000 N/rad
C_r	Cornering stiffness coefficients of rear tyres	95000 N/rad
k_1	Lift parameters from aerodynamics	0.005 N·s^2/m^2
k_2	Drag parameters from aerodynamics	0.41 N·s^2/m^2

4. Control design

The errors in position tracking are expressed as $x_e = x_d - x$ and $y_e = y_d - y$. The Euclidean distance error between the vehicle and the target point is defined as $L_e = \sqrt{x_e^2 + y_e^2}$. Formulate the desired heading angle aligned with the target position.

$$\psi_d = \arctan\left(\frac{y_e}{x_e}\right) + \frac{\pi}{2}\left[1 - \operatorname{sign}(x_e)\right]\operatorname{sign}(y_e) \tag{6}$$

Accordingly, we characterize the heading angle error using $\psi_e = \psi - \psi_d$. The control input for r is designed to drive the heading error ψ_e to zero, while the control input for T aims to asymptotically eliminate the L_e. The geometric relationship in the tracking dynamics is shown in Figure 1.

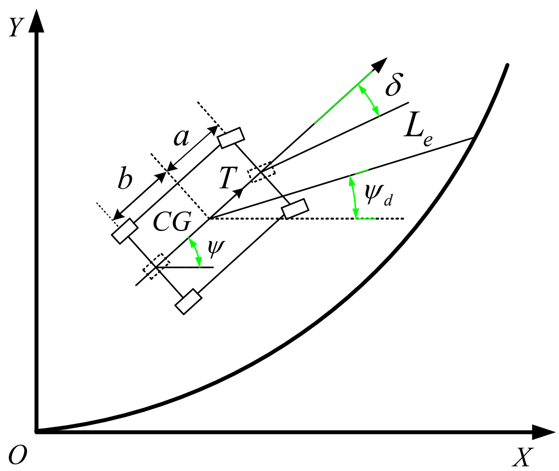

Figure 1. Schematic diagram of tracking dynamics.

Figure 1 sketches out the main control framework. There are two main modules in the system, namely the composite neural learning and the adaptive neural asymptotic control. The composite learning undertakes the training of NNs, which enhances their learning performance by involving the prediction errors generated by an adaptive asymptotic SPEM. The control module can generate the continuous control laws by employing the online trained NNs. The control laws therein are constructed in an adaptive asymptotic way. Then, the triggering conditions determine whether the continuous control signals are transmitted to the actuators of the actual car.

4.1. Control design in u

Step 1: By differentiating L_e based on the dynamics described in (5), we obtain:

$$\dot{L}_e = \cos\psi_d \dot{x}_d + \sin\psi_d \dot{y}_d - u\cos\psi_e + v\sin\psi_e \tag{7}$$

Design the virtual control input α_u as

$$\alpha_u = \frac{1}{\cos\psi_e}\left[k_L L_e + \cos\psi_d \dot{x}_d + \sin\psi_d \dot{y}_d + v\sin\psi_e\right] \tag{8}$$

where $k_L > 0$ denotes a tunable gain parameter. Define the velocity tracking error as $u_e = u - \alpha_u$. Substituting (8) into (7) yields:

$$\dot{L}_e = -k_L L_e - u_e \cos\psi_e \tag{9}$$

To analyze stability, consider the Lyapunov function candidate $V_L = L_e^2/2$. Taking its time derivative along the derivative of the distance error (7):

$$\dot{V}_L = -k_L L_e^2 - u_e \cos\psi_e L_e \tag{10}$$

Step 2: Differentiating u_e along with (5), it renders

$$\dot{u}_e = \frac{T}{m} + \mu_u - \dot{\alpha}_u \tag{11}$$

where $\mu_u = vr - fg + m^{-1}\left[(fk_1 - k_2)u^2 + C_f\delta(v + ar)u^{-1}\right]$, According to (8), it is known that

$$\dot{\alpha}_u = \frac{\partial\alpha_u}{\partial\psi_e}\dot{\psi}_e + \frac{\partial\alpha_u}{\partial L_e}\dot{L}_e + \frac{\partial\alpha_u}{\partial\psi_d}\dot{\psi}_d + \frac{\partial\alpha_u}{\partial v}\dot{v} + \frac{\partial\alpha_u}{\partial\dot{x}_d}\ddot{x}_d + \frac{\partial\alpha_u}{\partial\dot{y}_d}\ddot{y}_d \tag{12}$$

Invoking (1), it has

$$\mu_u - \dot{\alpha}_u - L_e\cos\psi_e = W_u^{\mathrm{T}}\varphi_u(s_u) + \varepsilon_u(s_u) \tag{13}$$

where $s_u = [x, y, \psi, x_d, \dot{x}_d, y_d, \dot{y}_d, \ddot{x}_d, \ddot{y}_d, u, v, r, \delta]^{\mathrm{T}}$. Inserting the expression from (13) into (11) leads to the following result:

$$\dot{u}_{\mathrm{e}} = \frac{T}{m} + W_u^{\mathrm{T}}\varphi_u(s_u) + \varepsilon_u(s_u) + L_e\cos\psi_e \tag{14}$$

Design the real control law of T:

$$T(t) = \omega_u(t_i^u), t \in (t_i^u, t_{i+1}^u] \tag{15}$$

where $\omega_u(t)$ is the continuous control law, t_i^u is the current triggering instant. The control error is written as $e_u(t) = \omega_u(t) - T(t)$. Then, we can obtain the triggering condition:

$$t_{i+1}^u = \{t > t_i^u \wedge |e_u| \geq a_u|T| + b_u\} \tag{16}$$

where $0 < a_u < 1$ and $b_u > 0$. The expression for $T(t)$ is written as

$$T(t) = \frac{\omega_u(t)}{(1+\xi_1 a_u)} - \frac{\xi_2 b_u}{(1+\xi_1 a_u)} \tag{17}$$

and (14) is transformed to

$$\dot{u}_\mathrm{e} = \frac{\omega_u(t)}{m(1+\xi_1\alpha_u)} - \frac{\xi_2 b_u}{m(1+\xi_1\alpha_u)} + W_u^\mathrm{T}\varphi_u(s_u) + \varepsilon_u(s_u) + L_e\cos\psi_e \tag{18}$$

where $\xi_1 \in (-1,1)$ and $\xi_2 \in (-1,1)$.

The prediction error is defined as

$$z_{uNN} = u_e - \hat{u}_e \tag{19}$$

where the derivative of NN modeling information is defined with the serial-parallel estimation model as

$$\dot{\hat{u}}_e = \frac{T}{m} + \hat{W}_u^\mathrm{T}\varphi_u(s_u) + L_e\cos\psi_e + \varsigma_u z_{uNN} + \frac{z_{uNN}\hat{\bar{\varepsilon}}_u}{\sqrt{z_{uNN}^2 + \sigma_u^2}} \tag{20}$$

where $\hat{u}_e(0) = u_e(0)$, with $\varsigma_u > 0$ as the user-defined positive constant. Select the Lyapunov candidate as$V_{uw} = \tilde{W}_u^\mathrm{T}\tilde{W}_u/2\gamma_u + \gamma_{zu}z_{uNN}^2/2$, $\hat{W}_u^\mathrm{T}$ is the estimate of W_u^T with $W_u^\mathrm{T} = \tilde{W}_u^\mathrm{T} + \hat{W}_u^\mathrm{T}$. Invoking$\dot{\hat{W}}_u = \dot{\tilde{W}}_u$, it renders

$$\dot{V}_{uw} = -\frac{1}{\gamma_u}\tilde{W}_u^\mathrm{T}\dot{\hat{W}}_u + \gamma_{zu}z_{uNN}\dot{z}_{uNN} \tag{21}$$

For the NN updating law and (3), the signal z_{uNN} is employed to construct the learning design

$$\dot{\hat{W}}_u = \gamma_u\left[(u_e + \gamma_{zu}z_{uNN})\varphi_u(s_u) - \sigma_u\hat{W}_u\right] \tag{22}$$

where γ_u and γ_{zu} are positive design constants. For the NN prediction error, using (19) and (20), we have

$$\dot{z}_{uNN} = \tilde{W}_u^\mathrm{T}\varphi_u(s_u) + \bar{\varepsilon}_u(s_u) - \varsigma_u z_{uNN} - \frac{z_{uNN}\hat{\bar{\varepsilon}}_u}{\sqrt{z_{uNN}^2 + \sigma_u^2}} \tag{23}$$

By substituting (22), (23) to (21), it renders

$$\begin{aligned}\dot{V}_{uw} =& -\tilde{W}_u^{\mathrm{T}}\left[\left(u_e+\gamma_{zu}z_{uNN}\right)\varphi_u\left(s_u\right)-\sigma_u\hat{W}_u\right]\\&+z_{uNN}\left[\tilde{W}_u^{\mathrm{T}}\varphi_u\left(s_u\right)+\bar{\varepsilon}_u\left(s_u\right)-\varsigma_u z_{uNN}-\frac{z_{uNN}\hat{\bar{\varepsilon}}_u}{\sqrt{z_{uNN}^2+\sigma_u^2}}\right]\end{aligned} \tag{24}$$

Based on Lemma 3 and Lemma 1, we can derive

$$z_{uNN}\bar{\varepsilon}_u \leq \frac{z_{uNN}^2\bar{\varepsilon}_u}{\sqrt{z_{uNN}^2+\sigma_u^2}}+\sigma_u\bar{\varepsilon}_u \tag{25}$$

$\hat{\bar{\varepsilon}}_u$ is the estimate of $\bar{\varepsilon}_u$ with $\tilde{\bar{\varepsilon}}_u=\bar{\varepsilon}_u-\hat{\bar{\varepsilon}}_u$. By substituting (24) to (25), it renders

$$\dot{V}_{uw} \leq -W_u^{\mathrm{T}}\varphi_u\left(s_u\right)u_e-\varsigma_u z_{uNN}^2+\sigma_u\tilde{W}_u^{\mathrm{T}}\hat{W}_u-\frac{z_{uNN}^2\tilde{\bar{\varepsilon}}_u}{\sqrt{z_{uNN}^2+\sigma_u^2}}+\sigma_u\bar{\varepsilon}_u \tag{26}$$

Note that $\tilde{W}_u^{\mathrm{T}}\hat{W}_u=\tilde{W}_uW_u-\tilde{W}_u^{\mathrm{T}}\tilde{W}_u\leq W_u^{\mathrm{T}}W_u/4$, it renders

$$\dot{V}_{uw} \leq -W_u^{\mathrm{T}}\varphi_u\left(s_u\right)u_e-\varsigma_u z_{uNN}^2+\frac{\sigma_u W_u^2}{4}-\frac{z_{uNN}^2\tilde{\bar{\varepsilon}}_u}{\sqrt{z_{uNN}^2+\sigma_u^2}}+\sigma_u\bar{\varepsilon}_u \tag{27}$$

Design the adaptive law of $\hat{\bar{\varepsilon}}_u$ as

$$\dot{\hat{\bar{\varepsilon}}}_u=\chi_u\frac{z_{uNN}^2}{\sqrt{z_{uNN}^2+\sigma_u^2}}-\chi_u\sigma_u\hat{\bar{\varepsilon}}_u \tag{28}$$

where $\chi_u>0$. We define the Lyapunov candidate as $V_{\tilde{\bar{\varepsilon}}_u}=\tilde{\bar{\varepsilon}}_u^2/(2\chi_u)$. Note that $\tilde{\bar{\varepsilon}}_u\hat{\bar{\varepsilon}}_u=\tilde{\bar{\varepsilon}}_u\bar{\varepsilon}_u-\tilde{\bar{\varepsilon}}_u^2\leq\bar{\varepsilon}_u^2/4$. Differentiating $V_{\tilde{\bar{\varepsilon}}_u}$ along with (28), it renders

$$\dot{V}_{\tilde{\bar{\varepsilon}}_u}\leq-\frac{\tilde{\bar{\varepsilon}}_u z_{uNN}^2}{\sqrt{z_{uNN}^2+\sigma_u^2}}+\frac{\bar{\varepsilon}_u^2}{4}\sigma_u \tag{29}$$

With the Lyapunov function candidate $V_u=u_e^2/2$, differentiation along the system described by (18) and (4), we obtain:

$$\dot{V}_u=\frac{\omega_u\left(t\right)u_e}{m\left(1+\xi_1\alpha_u\right)}-\frac{\xi_2 b_u u_e}{m\left(1+\xi_1\alpha_u\right)}+W_u^{\mathrm{T}}\varphi_u\left(s_u\right)u_e+\varepsilon_u u_e+L_e\cos\psi_e u_e \tag{30}$$

By considering $W_u^{\mathrm{T}}=\tilde{W}_u^{\mathrm{T}}+\hat{W}_u^{\mathrm{T}}$, it renders,

$$\dot{V}_u\leq\frac{\omega_u u_e}{m\left(1+\xi_1\alpha_u\right)}+\beta_u\left|u_e\right|+\hat{W}_u^{\mathrm{T}}\varphi_u\left(s_u\right)u_e+L_e\cos\psi_e u_e+\tilde{W}_u^{\mathrm{T}}\varphi_u\left(s_u\right)u_e \tag{31}$$

where $\beta_u = b_u/[m(1-\alpha_u)] + \bar{\varepsilon}_u$. According to Lemma 3,

$$\beta_u |u_e| \leq \frac{\beta_u u_e^2}{\sqrt{u_e^2 + \sigma_u^2}} + \beta_u \sigma_u \tag{32}$$

$$\hat{W}_u^{\mathrm{T}} \varphi_u |u_e| \leq \frac{\left(\hat{W}_u^{\mathrm{T}} \varphi_u\right)^2 u_e}{\sqrt{\left(\hat{W}_u^{\mathrm{T}} \varphi_u u_e\right)^2 + \sigma_u^2}} + \sigma_u \tag{33}$$

By substituting (32) and (33) to (31) , it renders

$$\begin{aligned} \dot{V}_u \leq & \frac{\omega_u u_e}{m(1+\xi_1 \alpha_u)} + \frac{\beta_u u_e^2}{\sqrt{u_e^2 + \sigma_u^2}} + \beta_u \sigma_u + L_e \cos \psi_e u_e \\ & + \frac{\left(\hat{W}_u^{\mathrm{T}} \varphi_u\right)^2 u_e}{\sqrt{\left(\hat{W}_u^{\mathrm{T}} \varphi_u u_e\right)^2 + \sigma_u^2}} + \tilde{W}_u^{\mathrm{T}} \varphi_u u_e + \sigma_u \end{aligned} \tag{34}$$

Let $\omega_u(t)$ be defined as:

$$\omega_u(t) = -m(1+a_u)\left[k_u u_e + \frac{\hat{\beta}_u u_e}{\sqrt{u_e{}^2 + \sigma_u^2}} + \frac{\left(\hat{W}_u^{\mathrm{T}} \varphi_u\right)^2 u_e}{\sqrt{\left(\hat{W}_u^{\mathrm{T}} \varphi_u u_e\right)^2 + \sigma_u^2}}\right] \tag{35}$$

where $k_u > 0$ and $\hat{\beta}_u$ denotes the estimate of β_u, where $\tilde{\beta}_u = \beta_u - \hat{\beta}_u$. Substituting (35) to (34) yields:

$$\dot{V}_u \leq -k_u u_e^2 + \frac{\tilde{\beta}_u u_e^2}{\sqrt{u_e^2 + \sigma_u^2}} + \beta_u \sigma_u + L_e \cos \psi_e u_e + \sigma_u + \tilde{W}_u^{\mathrm{T}} \varphi_u(s_u) u_e \tag{36}$$

Formulate the adaptive update law for $\hat{\beta}_u$ as follows:

$$\dot{\hat{\beta}}_u = \lambda_u \frac{u_e^2}{\sqrt{u_e^2 + \sigma_u^2}} - \lambda_u \sigma_u \hat{\beta}_u \tag{37}$$

where $\lambda_u > 0$ is the tuning parameter. Select the Lyapunov candidate as $V_{\tilde{\beta}_u} = \tilde{\beta}_u^2 \big/ (2\lambda_u)$. Note that $\tilde{\beta}_u \hat{\beta}_u = \tilde{\beta}_u \beta_u - \tilde{\beta}_u^2 \leq \beta_u^2/4$. Differentiating $V_{\tilde{\beta}_r}$ along with (29), it yields

$$\dot{V}_{\tilde{\beta}_u} \leq -\frac{\tilde{\beta}_u u_e^2}{\sqrt{u_e^2 + \sigma_u^2}} + \frac{\beta_u^2}{4} \sigma_u \tag{38}$$

4.2. Control design in r

Step 1: Differentiating ψ_e with respect to (5) gives:

$$\dot{\psi}_e = r - \dot{\psi}_d \tag{39}$$

We define the virtual control law α_r as:

$$\alpha_r = -k_\psi \psi_e + \dot{\psi}_d \tag{40}$$

where $k_\psi > 0$. Characterize the error in r tracking as $r_e = r - \alpha_r$. Substituting Equation (40) into (39) results in:

$$\dot{\psi}_e = -k_\psi \psi_e + r_e \tag{41}$$

We define the Lyapunov function as $V_\psi = \psi_e^2/2$, and we can get:

$$\dot{V}_\psi = -k_\psi \psi_e^2 + \psi_e r_e \tag{42}$$

Step 2: Differentiating r_e with respect to Equation (5) yields:

$$\dot{r}_e = \frac{a\delta\left(C_r + T\right)}{I_z} + \mu_r - \dot{\alpha}_r \tag{43}$$

where $\mu_r = I_z{}^{-1}\left[-fmhur + vu^{-1}\left(bC_r - aC_f\right) - ru^{-1}\left(b^2C_f + a^2C_r\right)\right]$. According to (40), it is known that

$$\dot{a}_r = \frac{\partial a_r}{\partial \psi_e}\dot{\psi}_e + \frac{\partial a_r}{\partial \phi_d}\ddot{\psi}_d \tag{44}$$

Invoking (1), it renders

$$\mu_r - \dot{\alpha}_r + \psi_e = W_r^{\mathrm{T}}\varphi_r(s_r) + \varepsilon_r(s_r) \tag{45}$$

where $s_r = [x, y, \psi, x_d, y_d, \dot{x}_d, \dot{y}_d, \ddot{x}_d, \ddot{y}_d, u, v, r, T, \delta]^{\mathrm{T}}$. Substituting (45) to (43), we can get

$$\dot{r}_e = \frac{a\delta\left(C_r + T\right)}{I_z} - \psi_e + W_r^{\mathrm{T}}\varphi_r\left(s_r\right) + \varepsilon_r\left(s_r\right) \tag{46}$$

Design the real control law of δ as

$$\delta\left(t\right) = \omega_r\left(t_i^r\right), t \in \left(t_i^r, t_{i+1}^r\right] \tag{47}$$

where ω_r is the continuous control law. The control error is written as $e_r\left(t\right) = \omega_r\left(t\right) - \delta\left(t\right)$. We obtain the triggering condition

$$t_{i+1}^r = \left\{t > t_i^r \wedge |e_r| \geq a_r\left|\delta(t)\right| + b_r\right\} \tag{48}$$

where $0 < a_r < 1$ and $b_r > 0$, and $\delta\left(t\right) = \omega_r\left(t\right)/\left(1 + \zeta_1 a_r\right) - \zeta_2 b_r/\left(1 + \zeta_1 a_r\right)$. Thus, (46) can be rewritten as

$$\dot{r}_e = \frac{a\left(C_r + T\right)\omega_r\left(t\right)}{I_z\left(1 + \zeta_1 a_r\right)} - \frac{a\left(C_r + T\right)\zeta_2 b_r}{I_z\left(1 + \zeta_1 a_r\right)} + W_r^{\mathrm{T}}\varphi_r\left(s_r\right) + \varepsilon_r\left(s_r\right) - \psi_e \tag{49}$$

where $\zeta_1 \in (-1, 1)$ and $\zeta_2 \in (-1, 1)$.
The prediction error is defined as

$$z_{rNN} = r_e - \hat{r}_e \tag{50}$$

where the derivative of NN modeling information is defined with the serial-parallel estimation model.

$$\dot{\hat{r}}_e = \frac{a\delta\left(C_r + T\right)}{I_z} + \hat{W}_r^{\mathrm{T}}\varphi_r\left(s_r\right) - \psi_e + \varsigma_r z_{rNN} + \frac{z_{rNN}\hat{\bar{\varepsilon}}_{rN}}{\sqrt{z_{rNN}^2 + \sigma_r^2}} \tag{51}$$

where $\hat{r}_e\left(0\right) = r_e\left(0\right)$, with $\varsigma_r > 0$ as the user-defined positive constant. Select the Lyapunov candidate as$V_{rw} = \tilde{W}_r^{\mathrm{T}}\tilde{W}_r/2\gamma_r + \gamma_{zr}z_{rNN}^2/2$, $\hat{W}_r^{\mathrm{T}}$ is the estimate of W_r^{T} with $W_r^{\mathrm{T}} = \tilde{W}_r^{\mathrm{T}} + \hat{W}_r^{\mathrm{T}}$. Invoking $\dot{\hat{W}}_r = \dot{\tilde{W}}_r$, it renders

$$\dot{V}_{rw} = -\frac{1}{\gamma_r}\tilde{W}_r^{\mathrm{T}}\dot{\hat{W}}_r + \gamma_{zr}z_{rNN}\dot{z}_{rNN} \tag{52}$$

For the NN updating law, the signal z_{rNN} is employed to construct the learning design.

$$\dot{\hat{W}}_r = \gamma_r\left[\left(r_e + \gamma_{zr}z_{rNN}\right)\varphi_r\left(s_r\right) - \sigma_r\hat{W}_r\right] \tag{53}$$

where γ_r and γ_{zr} are positive design constants. For the NN prediction error, using (46), (50) and (51), we have

$$\dot{z}_{rNN} = \tilde{W}_r^{\mathrm{T}}\varphi_r\left(s_r\right) + \varepsilon_r\left(s_r\right) - \varsigma_r z_{rNN} - \frac{z_{rNN}\hat{\bar{\varepsilon}}_{rN}}{\sqrt{{z_{rNN}}^2 + \sigma_r^2}} \tag{54}$$

By substituting (54), (53) to (52), it renders

$$\begin{aligned}\dot{V}_{rw} =& -\tilde{W}_r^{\mathrm{T}}\left[\left(r_e + \gamma_{zr}z_{rNN}\right)\varphi_r\left(s_r\right) - \sigma_r\hat{W}_r\right]\\ &+ z_{rNN}\left[\tilde{W}_r^{\mathrm{T}}\varphi_r\left(s_r\right) + \varepsilon_r\left(s_r\right) - \varsigma_r z_{rNN} - \frac{z_{rNN}\hat{\bar{\varepsilon}}_{rN}}{\sqrt{{z_{rNN}}^2 + \sigma_r^2}}\right]\end{aligned} \tag{55}$$

According to Lemma 3 and Lemma 1, it is known that

$$z_{rNN}\varepsilon_r\left(s_r\right) \le z_{rNN}\bar{\varepsilon}_{rN} \le \frac{z_{rNN}^2\bar{\varepsilon}_{rN}}{\sqrt{{z_{rNN}}^2 + \sigma_r^2}} + \sigma_r\bar{\varepsilon}_{rN} \tag{56}$$

$\hat{\bar{\varepsilon}}_{rN}$ is the estimate of $\bar{\varepsilon}_{rN}$ with $\tilde{\bar{\varepsilon}}_{rN} = \bar{\varepsilon}_{rN} - \hat{\bar{\varepsilon}}_{rN}$. By substituting (56) to (55), it renders

$$\dot{V}_{rw} \le -W_r^{\mathrm{T}}\varphi_r\left(s_r\right)r_e - \varsigma_r z_{rNN}^2 + \sigma_r\tilde{W}_r^T\hat{W}_r - \frac{z_{rNN}^2\tilde{\bar{\varepsilon}}_{rN}}{\sqrt{{z_{rNN}}^2 + \sigma_r^2}} + \sigma_r\bar{\varepsilon}_{rN} \tag{57}$$

Note that $\tilde{W}_r^{\mathrm{T}}\hat{W}_r = \tilde{W}_r W_r - \tilde{W}_r^{\mathrm{T}}\tilde{W}_r \le W_r^{\mathrm{T}}W_r/4$, it renders

$$\dot{V}_{rw} \le -W_r^{\mathrm{T}}\varphi_r\left(s_r\right)r_e - \varsigma_u z_{rNN}^2 + \frac{\sigma_r W_r^2}{4} - \frac{z_{rNN}^2\tilde{\bar{\varepsilon}}_{rN}}{\sqrt{z_{rNN}^2 + \sigma_r^2}} + \sigma_r\bar{\varepsilon}_{rN} \tag{58}$$

Design the adaptive law of $\hat{\bar{\varepsilon}}_{rN}$ as

$$\dot{\hat{\bar{\varepsilon}}}_{rN} = \chi_r \frac{z_{rNN}^2}{\sqrt{z_{rNN}^2 + \sigma_r^2}} - \chi_r \sigma_r \hat{\bar{\varepsilon}}_{rN} \tag{59}$$

where $\chi_r > 0$ is the tuning parameter. Select the Lyapunov candidate as $V_{\tilde{\bar{\varepsilon}}_{rN}} = \tilde{\bar{\varepsilon}}_{rN}^2/(2\chi_r)$. Note that $\tilde{\bar{\varepsilon}}_{rN}\hat{\bar{\varepsilon}}_{rN} = \tilde{\bar{\varepsilon}}_{rN}\bar{\varepsilon}_{rN} - \tilde{\bar{\varepsilon}}_{rN}^2 \leq \bar{\varepsilon}_{rN}^2/4$. Differentiating $V_{\tilde{\bar{\varepsilon}}_{rN}}$ along with (59), it renders

$$\dot{V}_{\tilde{\bar{\varepsilon}}_{rN}} \leq -\frac{\tilde{\bar{\varepsilon}}_{rN} z_{rNN}^2}{\sqrt{z_{rNN}^2 + \sigma_r^2}} + \frac{\bar{\varepsilon}_{rN}^2}{4}\sigma_r \tag{60}$$

With the Lyapunov function candidate $V_r = r_e^2$, differentiation along the system described by (49) gives:

$$\dot{V}_r = \frac{a(C_r+T)\omega_r(t)r_e}{I_z(1+\zeta_1 a_r)} - \frac{a(C_r+T)\zeta_2 b_r r_e}{I_z(1+\zeta_1 a_r)} + W_r^{\mathrm{T}}\varphi_r(s_r)r_e + \varepsilon_r r_e - \psi_e r_e \tag{61}$$

To solve the "algebraic loop" problem arising in the following control design, it is inferred from Lemma 2 that $\|\varphi_r(s_r)\| \leq \|\varphi_r(\bar{s}_r)\|$ where $\bar{s}_r = [x, y, \psi, x_d, y_d, \dot{x}_d, \dot{y}_d, \ddot{x}_d, \ddot{y}_d, u, v, r, T]^{\mathrm{T}}$. Invoking $W_r{}^{\mathrm{T}} = \tilde{W}_r^{\mathrm{T}} + \hat{W}_r^{\mathrm{T}}$, it renders

$$\begin{aligned}\dot{V}_r \leq & \frac{a(C_r+T)\omega_r r_e}{(1+\xi_1 a_r)I_z} - \frac{a(C_r+T)\zeta_2 b_r r_e}{I_z(1+\zeta_1 a_r)} - \psi_e r_e + \bar{\varepsilon}_r|r_e| \\ & + \|\hat{W}_r\| * \|\varphi_r(\bar{s}_r)\| * |r_e| + \tilde{W}_r^{\mathrm{T}}\varphi_r(s_r)r_e\end{aligned} \tag{62}$$

According to the actual situation, it has $|C_r + T| \neq 0$. By substituting (4) to (62), it has

$$\begin{aligned}\dot{V}_r \leq & \frac{a(C_r+T)\omega_r r_e}{I_z(1+\xi_1 a_r)} + \frac{\bar{\varepsilon}_r r_e^2}{\sqrt{r_e{}^2 + \sigma_r^2}} - \psi_e r_e + \bar{\varepsilon}_r \sigma_r \\ & + \frac{a\sigma_r}{I_z(1+\zeta_1 a_r)} + \frac{\hat{W}_r^{\mathrm{T}}\hat{W}_r\varphi_r^{\mathrm{T}}\varphi_r r_e^2}{\sqrt{\hat{W}_r^{\mathrm{T}}\hat{W}_r\varphi_r^{\mathrm{T}}\varphi_r r_e^2 + \sigma_r^2}} + \tilde{W}_u^{\mathrm{T}}\varphi_r r_e \\ & + \sigma_r + \frac{a}{I_z(1+\zeta_1 a_r)} \frac{(C_r+T)^2 b_r^2 r_e^2}{\sqrt{(C_r+T)^2 b_r^2 r_e^2 + \sigma_r^2}}\end{aligned} \tag{63}$$

Then, $\omega_r(t)$ can be written as

$$\begin{aligned}\omega_r(t) = & -\frac{I_z(1+a_r)}{a(C_r+T)}\left[k_r r_e + \frac{\hat{W}_r^{\mathrm{T}}\hat{W}_r\varphi_r^{\mathrm{T}}\varphi_r r_e}{\sqrt{\hat{W}_r^{\mathrm{T}}\hat{W}_r\varphi_r^{\mathrm{T}}\varphi_r r_e^2 + \sigma_r^2}}\right. \\ & \left. + \frac{\hat{\bar{\varepsilon}}_r r_e}{\sqrt{r_e^2 + \sigma_r^2}}\right] - \frac{(C_r+T)b_r^2 r_e}{\sqrt{(C_r+T)^2 b_r^2 r_e^2 + \sigma_r^2}}\end{aligned} \tag{64}$$

where $k_r > 0$, and $\tilde{\bar{\varepsilon}}_r = \bar{\varepsilon}_r - \hat{\bar{\varepsilon}}_r$. By substituting (64) to (63), it renders

$$\dot{V}_r \leq -k_r r_e^2 + \frac{\tilde{\bar{\varepsilon}}_r r_e^2}{\sqrt{r_e^2+\sigma_r^2}} + \bar{\varepsilon}_r \sigma_r - \psi_e r_e + \frac{a\sigma_r}{I_z(1+\zeta_1 a_r)} + \tilde{W}_r^T \varphi_r r_e + \sigma_r \tag{65}$$

The adaptive law of $\hat{\bar{\varepsilon}}_r$ can be designed as

$$\dot{\hat{\bar{\varepsilon}}}_r = \lambda_r \frac{r_e^2}{\sqrt{r_e^2+\sigma_r^2}} - \lambda_r \sigma_r \hat{\bar{\varepsilon}}_r \tag{66}$$

where $\lambda_r > 0$ is the tuning parameter. Select the Lyapunov candidate as $V_{\tilde{\bar{\varepsilon}}_r} = \tilde{\bar{\varepsilon}}_r^2/(2\lambda_r)$. Note that $\tilde{\bar{\varepsilon}}_r \hat{\bar{\varepsilon}}_r = \tilde{\bar{\varepsilon}}_r \bar{\varepsilon}_r - \tilde{\bar{\varepsilon}}_r^2 \leq \bar{\varepsilon}_r^2/4$. Differentiating $V_{\tilde{\bar{\varepsilon}}_r}$ along with (66), it renders

$$\dot{V}_{\tilde{\bar{\varepsilon}}_r} \leq -\frac{\tilde{\bar{\varepsilon}}_r r_e^2}{\sqrt{r_e^2+\sigma_r^2}} + \frac{\bar{\varepsilon}_r^2}{4}\sigma_r \tag{67}$$

Algorithmic implementation of the proposed control scheme is demonstrated as the flow chart in Table 2. In reality, t_s denotes the constant sampling step length of the processor, and j denotes the current accumulative sampling times. Thereby, the proposed scheme can be run in the control hardware.

Table 2. Pseudo codes of the proposed scheme.

Algorithm 1 ET-ACC

Initialize x, y, ψ, u, v, r, $\hat{W}_u$, $\hat{W}_r$, $\hat{\bar{\varepsilon}}_u$, $\hat{\bar{\varepsilon}}_{rN}$, $\hat{\beta}_u$, $\hat{\bar{\varepsilon}}_r$
For the computation time from $j = 1$ to $j = N$
for $j = 1$ to N **do**
    Calculate ω_u from (35) and ω_r from (64)
    if the triggering condition (16) is satisfied **then**
        Renew $t_i^u = t_0^u + j \cdot t_s$
        Update $T(t)$ by (15)
    end if
    if the triggering condition (48) is satisfied **then**
        Renew $t_i^r = t_0^r + j \cdot t_s$
        Update $\delta(t)$ by (47)
    end if
    Update $\hat{u}_e$ by (20)
    Update $\hat{r}_e$ by (51)
    Update $\hat{W}_u$ by (22)
    Update $\hat{W}_r$ by (53)
    Update $\hat{\bar{\varepsilon}}_u$ by (28)
    Update $\hat{\bar{\varepsilon}}_{rN}$ by (59)
    Update $\hat{\beta}_u$ by (37)
    Update $\hat{\bar{\varepsilon}}_r$ by (66)
    Execute $T(t)$ and $\delta(t)$ in the intelligent vehicle of (5)
end for

5. Stability analysis

The proposed control scheme is concluded as the following theorem:

Theorem 1. *For the intelligent vehicle described by (5), if Assumption 1 and Assumption 2 hold, the* *control laws in (15) and (47), the triggering conditions in (16) and (48), the NN updating law in (22) and (53), and the adaptive laws in (28), (37), (59) and (66) are applied, asymptotic stabilization of L_e and ψ_e is guaranteed.*

Proof: Select the resultant Lyapunov candidate as $V = V_L + V_\psi + V_u + V_r + V_{\tilde{\beta}_u} + V_{\tilde{\bar{\varepsilon}}_r} + V_{\tilde{\bar{\varepsilon}}_{rN}} + V_{rw} + V_{uw} + V_{\tilde{\bar{\varepsilon}}_u}$. By synthesizing (10), (27), (29), (36), (38), (42), (58), (60), (65) and (67), it can directly derive

$$\begin{aligned}\dot{V}_L \le & -k_L L_e^2 - k_u u_e^2 + \beta_u \sigma_u + \sigma_u + \frac{\beta_u^2}{4}\sigma_u - \varsigma_u z_{uNN}^2 \\ & + \frac{\sigma_u W_u^{\mathrm{T}} W_u}{4} + \sigma_u \bar{\varepsilon}_u + \frac{\bar{\varepsilon}_u^2}{4}\sigma_u - k_r r_e^2 - k_\psi \psi_e^2 + \bar{\varepsilon}_r \sigma_r \\ & + \frac{\bar{\varepsilon}_r^2}{4}\sigma_r + \frac{a\sigma_r}{I_z(1+\zeta_1 a_r)} + \frac{\bar{\varepsilon}_{rN}^2}{4}\sigma_r \\ & + \frac{\sigma_r W_r^{\mathrm{T}} W_r}{4} - \varsigma_r z_{rNN}^2 + \sigma_r\end{aligned} \tag{68}$$

Integrating both sides of (68) and invoking Lemma 3, it yields

$$\begin{aligned} V(t) - V(0) \le & \left(\beta_u + \frac{\beta_u^2}{4} + \frac{W_u^{\mathrm{T}} W_u}{4} + \bar{\varepsilon}_u + 1 + \frac{\bar{\varepsilon}_u^2}{4}\right)\bar{\sigma}_u \\ & - \int_0^t k_r r_e^2 + k_u u_e^2 + k_L L_e^2 + k_\psi \psi_e^2 + \varsigma_u z_{uNN}^2 + \varsigma_r z_{rNN}^2 dt \\ & + \left(\bar{\varepsilon}_r + \frac{\bar{\varepsilon}_r^2}{4} + \frac{a}{I_z(1+\zeta_1 a_r)} + \frac{\bar{\varepsilon}_{rN}^2}{4} + \frac{\sigma_r W_r^{\mathrm{T}} W_r}{4} + 1\right)\bar{\sigma}_r \end{aligned} \tag{69}$$

From (69), it can be inferred that $V(t) - V(0)$ is bounded. By rearranging the terms, (69) is rewritten as:

$$\begin{aligned} & \int_0^t k_r r_e^2 + k_u u_e^2 + k_L L_e^2 + k_\psi \psi_e^2 + \varsigma_u z_{uNN}^2 + \varsigma_r z_{rNN}^2 dt \\ & \le V(0) - V(t) + \left(\beta_u + \frac{{\beta_u}^2}{4} + \frac{W_u^{\mathrm{T}} W_u}{4} + \bar{\varepsilon}_u + 1 + \frac{\bar{\varepsilon}_u^2}{4}\right)\bar{\sigma}_u \\ & + \left(\bar{\varepsilon}_r + \frac{\bar{\varepsilon}_r^2}{4} + \frac{a}{I_z(1+\zeta_1 a_r)} + \frac{\bar{\varepsilon}_{rN}^2}{4} + \frac{\sigma_r W_r^{\mathrm{T}} W_r}{4} + 1\right)\bar{\sigma}_r \end{aligned} \tag{70}$$

Therefore, by applying Barbalat's lemma, it follows that $L_e \to 0$ and $\psi_e \to 0$ as shown in (70). The proof is completed.

Remark 2. *It is observed from (70) that the larger k_L, k_ψ, k_u and k_r will lead to the faster convergence of L_e and ψ_e but the larger energy cost and the shorter inter-event time. Although the inter-event time can be prolonged by tuning up a_u, a_r, b_u and b_r in (16) and (48), it will cost more energy as a_u and a_r are involved in the control laws of (35) and (64).*

6. Numerical experiment

The model of intelligent vehicle in [58] is selected for test and the value of parameters in model has been described in Table 1.

6.1. Round trajectory

In a round trajectory, the coordinates of the reference position are defined as $x_d(t) = 15 + 10\sin\left(2\pi t/50\right) - 15\exp(-t)$ and $y_d(t) = 15 - 10\cos\left(2\pi t/50\right)$. $\psi(0) = 45^\circ$ and all the other initial states of the intelligent vehicle are set as zeros. To approximate the model uncertainties, an RBF NN with 11 neurons is adopted in the experiment. In the proposed asymptotic tracking control scheme, the control parameters are set as

$$\begin{aligned} & k_u = 3, k_\psi = 8, k_L = 0.5, k_r = -5, a_u = 0.5, \\ & a_r = 0.1, \varsigma_u = \varsigma_r = 0.5, b_r = 0.05, b_u = 0.1, \\ & \sigma_u = \sigma_r = 0.5\exp(-0.02t) \end{aligned} \tag{71}$$

To demonstrate high-precision tracking performance of the proposed algorithm, To facilitate comparison, we adopt the robust damping control scheme outlined in [59], which is marked as RDC for brevity. This method was excused from the adaptive neural design by using the robust control gains, such that the computational complexity was reduced to the most. Its control gains k_u, k_ψ, k_L and k_r keep same with (71). To demonstrate the exquisite neural learning performance of the proposed scheme, the proposed scheme can be remade in the manner of DAC [47], which is marked as ET-DAC in the experiment. This comparison differed from the proposed scheme in its adaptive laws, which was absent from the considerations on asymptotical stability and composite neural learning. The proposed event-triggered asymptotic composite control scheme is abbreviated to ET-ACC for brevity. For the tracking experiment in 50 s, the experimental results are shown as follows.

To evaluate the control performance comprehensively, we define the indices of mean tracking errors (MTE) and mean control inputs (MCI) as follows:

$$\begin{aligned} & \mathrm{MTE}\cdot L_e = \frac{\int_5^{50} L_e \mathrm{d}t}{45}, \ \mathrm{MTE}\cdot \psi_e = \frac{\int_5^{50} |\psi_e| \mathrm{d}t}{45} \\ & \mathrm{MCI}\cdot T = \frac{\int_5^{50} |T| \mathrm{d}t}{45}, \ \mathrm{MCI}\cdot \delta = \frac{\int_5^{50} |\delta| \mathrm{d}t}{45} \end{aligned} \tag{72}$$

To bypass the overshoot at the initial stage, the indexes in (72) are calculated from 5 s instead of 0 s. Moreover, the computation time is recorded as CT and the memory occupancy as MO, which can evaluate the computational complexity of these control schemes. Setting the minimum running period as 0.01 s, the total sampling times of control inputs are recorded as $\mathrm{TST}\cdot T$ and $\mathrm{TST}\cdot \delta$. With such the hardware configuration (CPU:Intel Core i7-10875H 2.3GHz, RAM: 16.0GB) in the numerical experiment, the records of these indexes are provided in Table 3.

Table 3. Records of indexes for round trajectory.

Indexes	ET-ACC	ET-DAC in [47]	RDC in [59]
MTE $\cdot L_e$	0.103 m	1.782 m	3.265 m
MTE $\cdot \psi_e$	0.042 rad	0.053 rad	0.245 rad
MCI $\cdot T$	859.486 N	660.690 N	664.937 N
MCI $\cdot \delta$	0.067 rad	0.068 rad	0.056 rad
CT	1.835 s	1.265 s	0.904 s
MO	78522 kB	69707 kB	11258 kB
TST $\cdot T$	163	88	5000
TST $\cdot \delta$	357	322	5000

It is shown in Figure 2 that all the three schemes can avail the convergence of the intelligent vehicle to the reference path. However, it is inferred from Figure 3 that the proposed ETC-ACC scheme has the smaller steady tracking errors and the faster tracking speed than the others. The smaller MTE $\cdot L_e$ of ETC-ACC in Table 3 can also confirm this fact. Figure 4 exhibits the evolution of T and δ under three control schemes. The intermittent sampling in the ETC schemes can be clearly observed from the local view. According to MCI $\cdot T$ and MCI $\cdot \delta$ in Table 3, there is no much difference in energy cost between three schemes. Figure 5 illustrates the changes in inter-event time. For T, there are 163 triggering instants with inter-event times ranging from 0.01 s to 7.76 s, and 357 triggering instants with inter-event times varying between 0.01 s and a maximum of 3.57 s for δ. In contrast, there were 5000 sampling times in both control inputs of the time-triggered RDC scheme. Define $f_u = \mu_u - \dot{\alpha}_u - L_e \cos\phi_e$ in (13) and $f_r = \mu_r - \dot{\alpha}_r + \psi_e$ in (45). Figure 6 displays the approximation of $\hat{W}_u^{\mathrm{T}} \varphi_u(s_u)$ to f_u, and Figure 7 displays the approximation of $\hat{W}_r^{\mathrm{T}} \varphi_r(s_r)$ to f_r. By the merit of composite learning, the proposed ETC-ACC presents the better learning of NNs than the direct adaptive control in ETC-DAC. Consequently, the proposed ETC-ACC has the better tracking performance than the ETC-DAC in Figure 2 and Figure 3. Figure 8 gives the evolution of neural weights in ETC-ACC and ETC-DAC. It is observed from their 2-norms that all these weights tend to stable values. In view of computational complexity, it is observed from CT and MO in Table 3 that RDC is the most succinct one without adaptive parameters, ETC-ACC and ETC-DAC have the similar performance for involving the NNs.

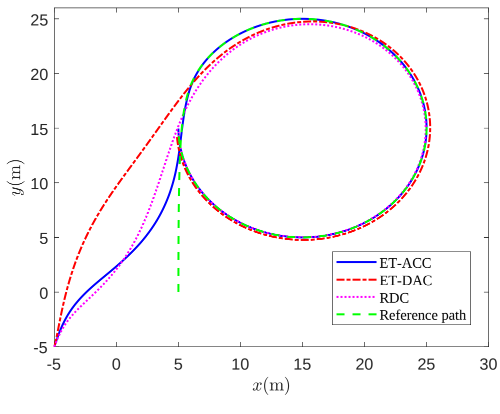

Figure 2. Trajectories of the intelligent vehicle under ETC-ACC, ET-DAC and RDC.

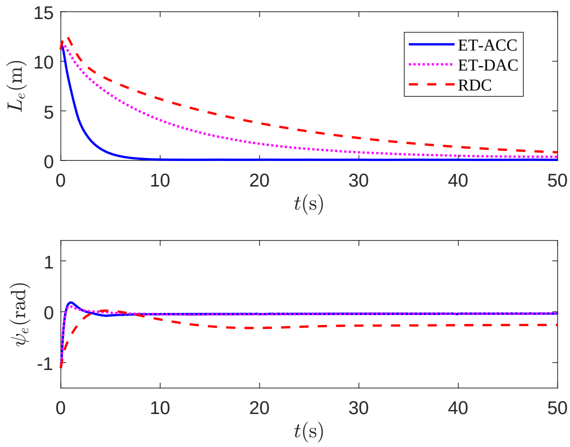

Figure 3. Tracking errors L_e and ψ_e under ETC-ACC, ET-DAC and RDC.

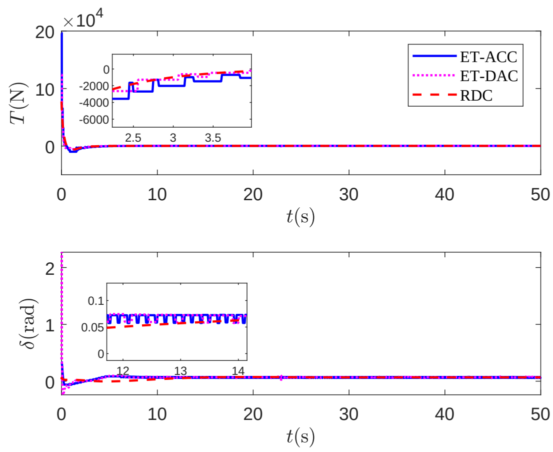

Figure 4. Control inputs T and δ under ETC-ACC, ET-DAC and RDC.

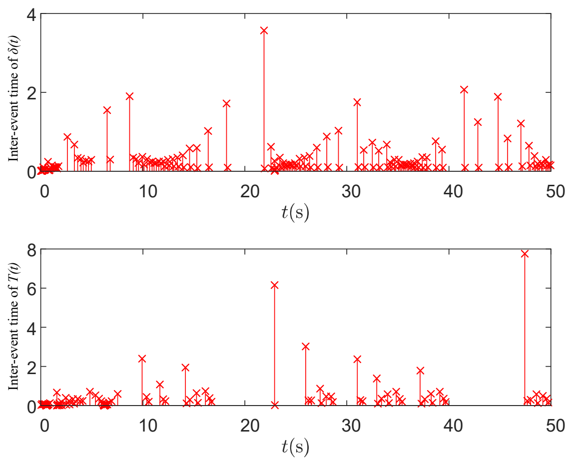

Figure 5. Inter-event time of ETC-ACC.

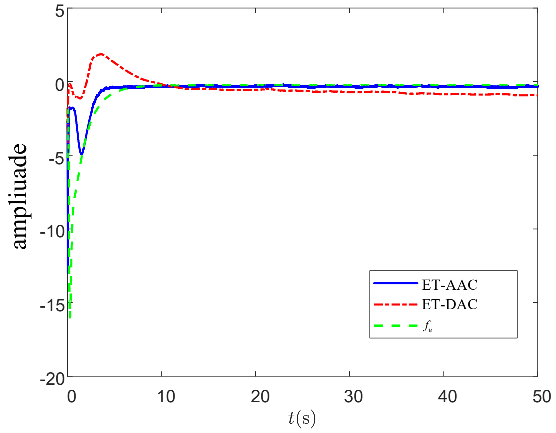

Figure 6. Approximation of NNs to f_u under ETC-ACC and ETC-DAC.

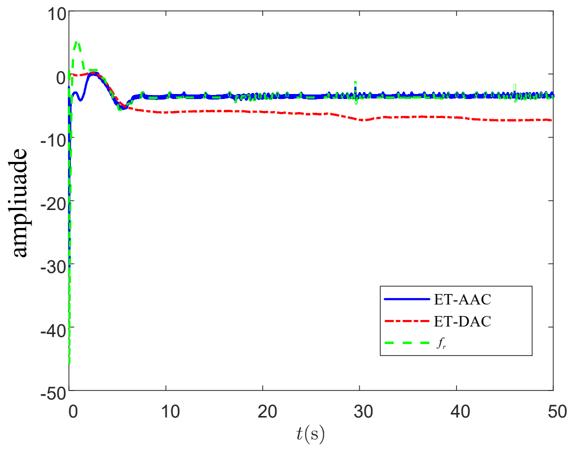

Figure 7. Approximation of NNs to f_r under ETC-ACC and ETC-DAC.

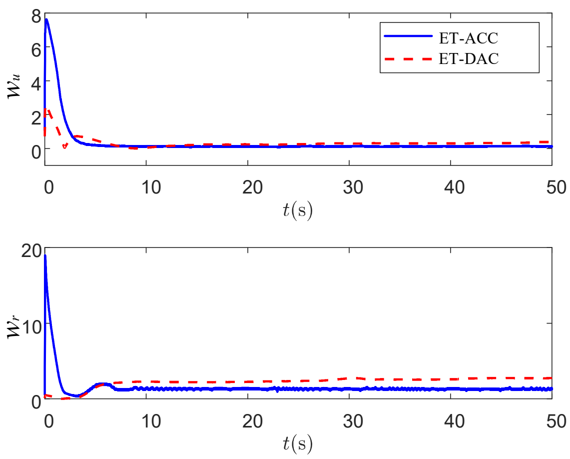

Figure 8. Update of neural weights $w_u = \|\hat{W}_u\|$ and $w_r = \|\hat{W}_r\|$ for ETC-ACC and ETC-DAC.

6.2. Trajectory with sudden transitions

To validate the performance of the proposed algorithm under sudden road transitions, we designed a scenario with abrupt transitions. The reference path trajectory is (73).

$$\begin{cases} x_d = 2t, y_d = 5, & \text{if } t < 50s \\ x_d = 2t, y_d = 15 & \text{else} \end{cases} \tag{73}$$

The total simulation time is 100 seconds in this case. Initial position of the vehicle as well as the controller parameters are consistent with the round trajectory case described above. Figure 9 to Figure 13 present the simulation results, while the numerical comparison results are summarized in Table 4. Figure 9 illustrates the trajectories of ETC-ACC and RDC algorithms under a sudden road change. By analyzing Figure 10 in conjunction with the numerical results presented in Table 4, it can be observed that ETC-ACC maintains high-precision tracking performance even in the presence of abrupt road variations. Figure 11 presents the control inputs T and δ for both the ETC-ACC and RDC algorithms. Notably, while ETC-ACC achieves superior tracking performance, its energy consumption is slightly higher compared to RDC. Figure 12 shows the inter-event time of the ETC-ACC algorithm, which represents the time intervals between successive triggering events. Finally, Figure 13 presents the evolution of the adaptive laws over time, illustrating how the system parameters adjust dynamically to ensure robust performance and accurate tracking under varying conditions.

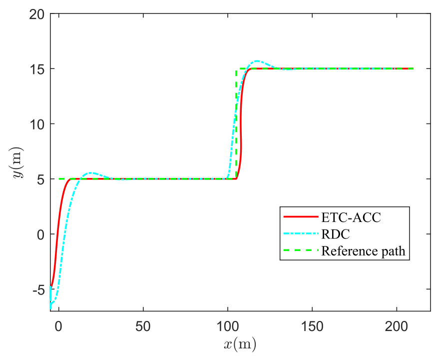

Figure 9. Trajectories of the intelligent vehicle under ETC-ACC and RDC.

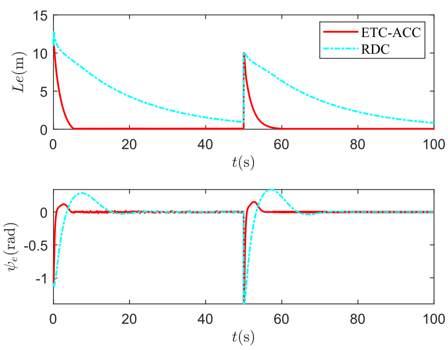

Figure 10. Tracking errors L_e and ψ_e under ETC-ACC and RDC.

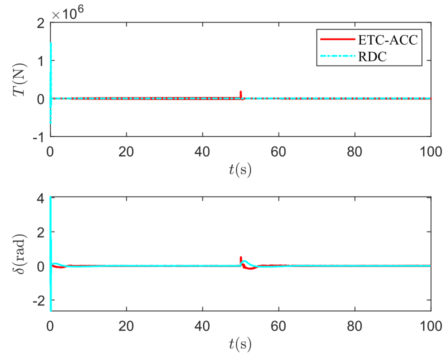

Figure 11. Control inputs T and δ under ETC-ACC and RDC.

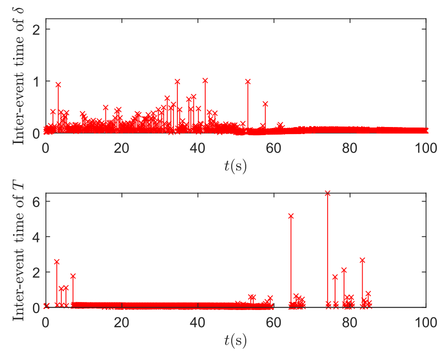

Figure 12. Inter-event time of ETC-ACC.

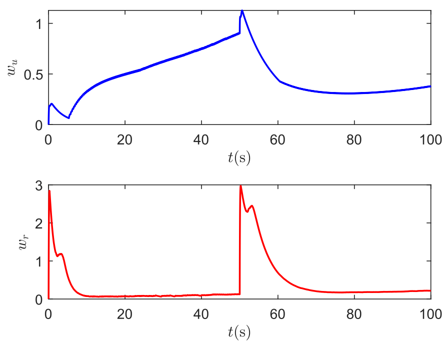

Figure 13. Update of neural weights $w_u = \|\hat{W}_u\|$ and $w_r = \|\hat{W}_r\|$ for ETC-ACC.

Table 4. Sudden transition trajectory index records.

Indexes	ET-ACC	RDC in [59]
MTE $\cdot L_e$	0.424 m	4.019 m
MTE $\cdot \psi_e$	0.0168 rad	0.0849 rad
MCI $\cdot T$	5789.33 N	871.16 N
MCI $\cdot \delta$	0.0135 rad	0.0170 rad

7. Conclusion

An event-triggered adaptive neural asymptotic tracking control scheme was developed for the intelligent vehicles. Through the numerical experiment, it was proved that the proposed scheme is more capable of high-precision tracking tasks by wielding the asymptotic stability and the composite learning of NNs. The event-triggered mechanism was independently taken in both the control inputs of T and δ, so as to alleviate the communication burden. The proposed scheme offered a uniform control framework for the nonlinear intelligent vehicles, which had wide practicability and high efficiency. One limitation of this study is that the proposed control framework does not explicitly account for external disturbances, such as wind gusts, sensor noise, and parameter variations, which may affect the real-world implementation of the control strategy. While the adaptive neural network compensates for system nonlinearities, its robustness against sudden and unpredictable disturbances has not been rigorously analyzed. Future research will focus on extending the proposed approach by incorporating disturbance observers or robust control techniques to enhance its resilience.

Acknowledgments

This work is partially supported by the Natural Science Foundation of China (No.52204404, No.U24A6008), the Hebei Province Natural Science Fund (No.E2024203179, E2022203088), the Science and Technology Project of Hebei Education Department (No.BJ2025114), and the Innovation Capacity Enhancement Program of Hebei Province (No.24461901D).

Author's contribution

Conceptualization, Yingjie Deng; software, Songtao Wang; validation, Tao Ni; formal analysis, Fangcheng Liu; writing—original draft preparation, Fangcheng Liu, Songtao Wang; writing—review and editing, Yingjie Deng, Yifei Xu, Tao Ni, Dingxuan Zhao; supervision, Yifei Xu; funding acquisition, Dingxuan Zhao. All authors have read and agreed to the published version of the manuscript.

Conflicts of interests

The authors declared that they have no conflicts of interests.

References

[1] Milani S, Khayyam H, Marzbani H, Melek W, Azad NL, *et al.* Smart autodriver algorithm for real-time autonomous vehicle trajectory control. *IEEE Trans. Intell. Transp. Syst.* 2022, 23(3):1984–1995.

[2] Narendran VK, Hedrick JK. Autonomous lateral control of vehicles in an automated highway system. *Veh. Syst. Dyn.* 1994, 23(1):307–324.

[3] Hwang CL, Yang CC, Hung JY. Path tracking of an autonomous ground vehicle with different

payloads by hierarchical improved fuzzy dynamic sliding-mode control. *IEEE Trans. Fuzzy Syst.* 2018, 26(2):899–914.

[4] Zhang X, Zhu X. Autonomous path tracking control of intelligent electric vehicles based on lane detection and optimal preview method. *Expert Syst. Appl.* 2019, 121:38–48.

[5] Zou SC, Zhao WZ, Wang CY. Tracking and synchronization control strategy of vehicle dual-motor steer-by-wire system via super-twisting SOSMC and MDCS. *Mech. Syst. Signal Process.* 2023, 183:109638.

[6] Raffo GV, Gomes GK, Normey-Rico JE, Kelber CR, Becker LB. A predictive controller for autonomous vehicle path tracking. *IEEE Trans. Intell. Transp. Syst.* 2009, 10(1):92–102.

[7] Hu J, Xiong S, Zha J, Fu C. Lane detection and trajectory tracking control of autonomous vehicle based on model predictive control. *Int. J. Automot. Technol.* 2020, 21(2):285–295.

[8] Berntorp K, Quirynen R, Uno T, Cairano SD. Trajectory tracking for autonomous vehicles on varying road surfaces by friction-adaptive nonlinear model predictive control. *Veh. Syst. Dyn.* 2019, 58(5):705–725.

[9] Hu C, Jing H, Wang RR, Yan FJ, Chadli M. Robust H_∞ output-feedback control for path following of autonomous ground vehicles. *Mech. Syst. Signal Process.* 2016, 70–71:414–427.

[10] Wang R, Jing H, Hu C, Yan F, Chen N. Robust H_∞ path following control for autonomous ground vehicles with delay and data dropout. *IEEE Trans. Control Syst. Technol.* 2016, 17(7):2042–2050.

[11] Zhang W. A robust lateral tracking control strategy for autonomous driving vehicles. *Mech. Syst. Signal Process.* 2021, 150:107238.

[12] Wang H, Song WW, Liang YY, Li Q, Liang DY. Observer-based finite frequency H_∞ state-feedback control for autonomous ground vehicles. *ISA Trans.* 2022, 121:75–85.

[13] Li W, Xie Z, Zhao J, Wong PK. Velocity-based robust fault tolerant automatic steering control of autonomous ground vehicles via adaptive event triggered network communication. *Mech. Syst. Signal Process.* 2020, 143:106798.

[14] Jiang Y, Xu XJ, Zhang L. Heading tracking of 6WID/4WIS unmanned ground vehicles with variable wheelbase based on model free adaptive control. *Mech. Syst. Signal Process.* 2021, 159:107715.

[15] Chen B, Zhang H, Liu X, Lin C. Neural observer and adaptive neural control design for a class of nonlinear systems. *IEEE Trans. Neural Networks Learn. Syst.* 2018, 29(9):4261–4271.

[16] Li Y, Shao X, Tong S. Adaptive fuzzy prescribed performance control of nontriangular structure nonlinear systems. *IEEE Trans. Fuzzy Syst.* 2020, 28(10):2416–2426.

[17] Liu Z, Shi P, Chen B, Lin C. Control design for uncertain switched nonlinear systems: adaptive neural approach. *IEEE Trans. Syst. Man Cybern.: Syst.* 2021, 51(4):2322–2331.

[18] Qin Y, Cao L, Ren H, Liang H, Pan Y. Adaptive optimal backstepping control for strict-feedback nonlinear systems with time-varying partial output constraints. *J. Franklin Inst.* 2024, 361(2):776–795.

[19] Yang W, Wang QG, Liu J, Yu J. Actor–Critic-Based Predefined-Time Fuzzy Adaptive Optimal Control for Uncertain Nonlinear Systems With Input Saturation. *IEEE Trans. Fuzzy Syst.* 2024, 32(4):2448–2457.

[20] Kumarawadu S, Lee TT. Neuroadaptive combined lateral and longitudinal control of highway

vehicles using RBF networks. *IEEE Trans. Intell. Transp. Syst.* 2006, 7(4):500–512.

[21] Zhang C, Hu J, Qiu J, Yang W, Sun H, *et al.* A novel fuzzy observer-based steering control approach for path tracking in autonomous vehicles. *IEEE Trans. Fuzzy Syst.* 2019, 27(2):278–290.

[22] Chu Z, Zhu D, Yang SX. Observer-based adaptive neural network trajectory tracking control for remotely operated vehicle. *IEEE Trans. Neural Networks Learn. Syst.* 2017, 28(7):1633–1645.

[23] Deng Y, Zhang X, Im N, Zhang G, Zhang Q. Model-based event-triggered tracking control of underactuated surface vessels with minimum learning parameters. *IEEE Trans. Neural Networks Learn. Syst.* 2020, 31(10):4001–4014.

[24] Xu B, Shi Z, Yang C, Sun F. Composite neural dynamic surface control of a class of uncertain nonlinear systems in strict-feedback form. *IEEE Trans. Cybern.* 2014, 44(12):2626–2634.

[25] Liu L, Wang D, Peng Z. Path following of marine surface vehicles with dynamical uncertainty and time-varying ocean disturbances. *Neurocomputing* 2016, 173:799–808.

[26] Pan Y, Yu H. Composite learning robot control with guaranteed parameter convergence. *Automatica* 2018, 89:398–406.

[27] Xu B, Shou Y, Luo J, Pu H, Shi Z. Neural learning control of strict-feedback systems using disturbance observer. *IEEE Trans. Neural Networks Learn. Syst.* 2019, 30(5):1296–1307.

[28] Guo K, Pan Y, Zhang D, Yu H. Composite learning control of robotic systems: a least squares modulated approach. *Automatica* 2020, 111:108612.

[29] Liu J, Du J. Composite learning tracking control for underactuated autonomous underwater vehicle with unknown dynamics and disturbances in three-dimension space. *Appl. Ocean Res.* 2021, 112:102686.

[30] Huang J, Hung T, Tseng M. Smooth switching robust adaptive control for omnidirectional mobile robots. *IEEE Trans. Control Syst. Technol.* 2015, 23(5):1986–1994.

[31] Lu H, Xie X, Chen P. Relaxed conditions of observer design of discrete-time takagi-sugeno fuzzy systems via a new multi-instant gain-scheduling scheme. *IEEE Trans. Fuzzy Syst.* 2022, 30(7):2759–2768.

[32] Ding F, Li Q, Jiang C, Han X, Liu J, *et al.* Event-triggered control for nonlinear leaf spring hydraulic actuator suspension system with valve predictive management. *Inf. Sci.* 2021, 551:184–204.

[33] Zhang Z, Xu S, Zhang B. Asymptotic tracking control of uncertain nonlinear systems with unknown actuator nonlinearity. *IEEE Trans. Autom. Control* 2014, 59(5):1336–1341.

[34] Li Y, Yang G. Adaptive asymptotic tracking control of uncertain nonlinear systems with input quantization and actuator faults. *Automatica* 2016, 72:177–185.

[35] Wu L, Park JH, Xie X, Li Y. Adaptive asymptotic tracking control of uncertain nonlinear systems based on Taylor decoupling and event-trigger. *IEEE Trans. Syst. Man Cybern.: Syst.* 2022, 52(4):2053–2060.

[36] Hu X, Long Y, Li T, Chen CLP. Adaptive fuzzy backstepping asymptotic disturbance rejection of multi-agent systems with unknown model dynamics. *IEEE Trans. Fuzzy Syst.* 2022, 30(11):4775–4787.

[37] Liang Y, Li Y, Che W, Hou Z. Adaptive fuzzy asymptotic tracking for nonlinear systems with nonstrict-feedback structure. *IEEE Trans. Cybern.* 2021, 51(2):853–861.

[38] Liu Y, Zhu Q. Adaptive neural network asymptotic tracking control for nonstrict feedback stochastic nonlinear systems. *Neural Networks* 2021, 143:283–290.

[39] Zhang J, Niu B, Wang D, Wang H, Zhao P, *et al.* Time-/Event-triggered adaptive neural asymptotic tracking control for nonlinear systems with full-state constraints and application to single-link robot. *IEEE Trans. Neural Networks Learn. Syst.* 2021, 33(11):6690–6700.

[40] Cheng T, Niu B, Zhang J, Wang D, Wang Z. Time-/Event-triggered adaptive neural asymptotic tracking control of nonlinear interconnected systems with unmodeled dynamics and prescribed performance. *IEEE Trans. Neural Networks Learn. Syst.* 2021, 34(9):6557–6567.

[41] Niu B, Liu J, Wang D, Zhao X, Wang H. Adaptive decentralized asymptotic tracking control for large-scale nonlinear systems with unknown strong interconnections. *IEEE/CAA J. Autom. Sin.* 2022, 9(1):173–186.

[42] Deng Y, Zhang Z, Gong M, Ni T. Event-triggered asymptotic tracking control of underactuated ships with prescribed performance. *IEEE Trans. Intell. Transp. Syst.* 2022, 24(1):645–656.

[43] Xing L, Wen C, Liu Z, Su H, Cai J. Event-triggered adaptive control for a class of uncertain nonlinear systems. *IEEE Trans. Autom. Control* 2017, 62(4):2071–2076.

[44] Cao L, Zhou Q, Dong G, Li H. Observer-based adaptive event-triggered control for nonstrict-feedback nonlinear systems with output constraint and actuator failures. *IEEE Trans. Syst. Man Cybern.: Syst.* 2021, 51(3):1380–1391.

[45] Liu S, Zhang J, Zhang X, Yan H, Sun B. Event-triggered communication-based control for strict-feedback nonlinear systems. *IEEE Trans. Cybern.* 2022, 53(10):6376–6385.

[46] Deng Y, Zhao D, Chen B, Gong M. Double-channel event-triggered adaptie tracking control of nonstrict-feedback nonlinear systems. *J. Franklin Inst.* 2022, 359(13):7219–7232.

[47] Deng Y, Liu Z, Chen B. Event-triggered adaptive neural tracking control of nonstrict-feedback nonlinear systems with unknown measurement. *Nonlinear Dyn.* 2022, 109(2):863–875.

[48] Zhang G, Li J, Jin X, Liu C. Robust adaptive neural control for wing-sail-assisted vehicle via the multiport event-triggered approach. *IEEE Trans. Cybern.* 2021, 52(12):12916–12928.

[49] Jiao J, Wang G. Event triggered trajectory tracking control approach for fully actuated surface vessel. *Neurocomputing* 2016, 182:267–273.

[50] Zhang X, Yao S, Xing W, Feng Z. Fuzzy event-triggered sliding mode depth control of unmanned underwater vehicles. *Ocean Eng.* 2022, 266:112725.

[51] Wang Z, Tian X, Mai Q, Liu H. Fixed-time composite robust H_∞ tracking control of marine surface vessels based on the barrier Lyapunov function and an event-triggered strategy. *Ocean Eng.* 2022, 261:112113.

[52] Ahmad I, Ge X, Han Q. Decentralized dynamic event-triggered communication and active suspension control of in-wheel motor driven electric vehicles with dynamic damping. *IEEE/CAA J. Autom. Sin.* 2021, 8(5):971–986.

[53] Li W, Xie Z, Zhao J, Gao J, Hu Y, *et al.* Human-machine shared steering control for vehicle lane keeping systems via a fuzzy observer-based event-triggered method. *IEEE Trans. Intell. Transp. Syst.* 2022, 23(8):13731–13744.

[54] Liu X, Xu B, Shou Y, Fan Q, Chen Y. Event-triggered adaptive control of uncertain

nonlinear systems with composite condition. *IEEE Trans. Neural Networks Learn. Syst.* 2022, 33(10):6030–6037.

[55] Deng Y, Zhang X. Event-triggered composite adaptive fuzzy output feedback control for path following of autonomous surface vessels. *IEEE Trans. Fuzzy Syst.* 2021, 29(9):2701–2713.

[56] Zhu G, Ma Y, Li Z, Malekian R, Sotelo M. Dynamic event-triggered adaptive neural output feedback control for MSVs using composite learning. *IEEE Trans. Intell. Transp. Syst.* 2022, 24(1):787–800.

[57] Pan B, Chen C, Zhu G, Su Y. Event-triggered composite learning finite-time trajectory tracking control for underactuated MSVs subject to uncertainties. *IEEE Access* 2022, 10:14440–14449.

[58] Zhang J, Xu S, Richard A. Path tracking control of vehicles based on Lyapunov approach. In *Proceedings of the 2002 American Control Conference*, Anchorage, USA, May 8–10, 2002, pp. 2132–2137.

[59] Zhang G, Zhang X. Practical robust neural path following control for underactuated marine vessels with actuators uncertainties. *Asian J. Control* 2017, 19:173–187.